UiT
THE ARCTIC
UNIVERSITY
OF NORWAY

Faculty of Science and Technology
Department of Physics and Technology

# Estimation of power supply by renewable energy sources to a weather station at Nordlysobservatoriet, Alta

**Lars Marius Rannekleiv**

*EOM-3901 Master's Thesis in Energy, Climate and Enviroment*
*August 2019*

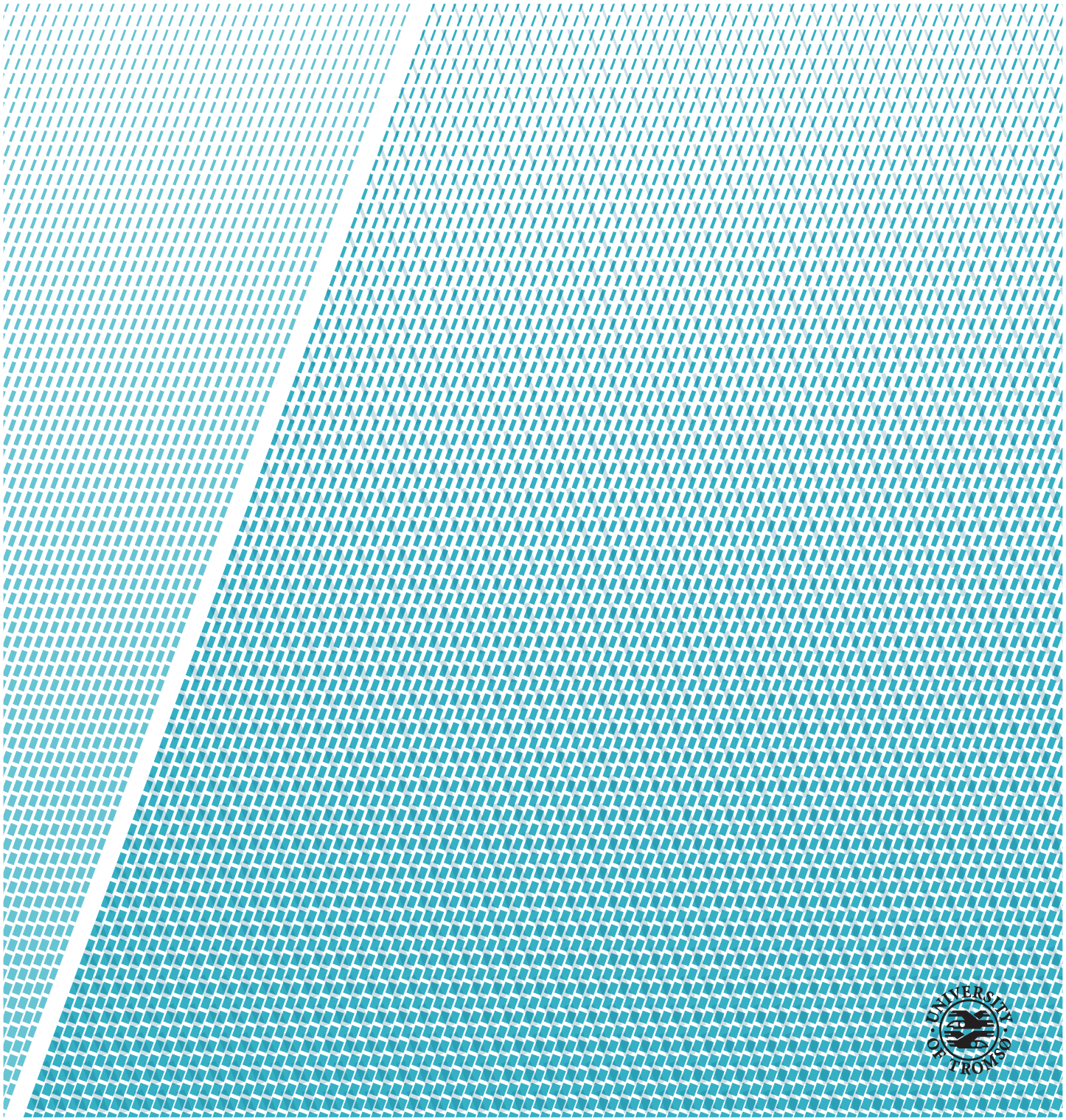

# Abstract

For a weather station that will be set up at Halddetoppen, Alta, there will also be installed a hybrid renewable energy system, to supply the station with power. This thesis simulated and estimated the hybrid system as it was planned, to see if it would be enough to give steady supply for the weather station. Different set-ups for the hybrid system was investigated. The set-ups differed in mounting of the solar photovoltaic panels, to see which placement of the panels would give the best and most secure power supply to the weather station. One set-up with only solar power, and one system with only wind power was also simulated. The system with only solar panels proved to be a poor power supply, as there's no solar radiation in the winter. The system with only wind turbines was found to be a better supply, but with fluctuations in wind energy, this system was found to be unsatisfactory. All the simulations with a hybrid system consisting of both wind turbines and solar panels was found to be satisfactory, and estimated to give a steady energy supply for the weather station.

# Acknowledgements

First of all, I would like to thank my supervisor, Associate professor Yngve Birkelund, for your guidance, ideas, and feedback for my thesis.

I would also wish to thank my fellow students for making the five year study period fun and intresting, as well as my family for supporting me through the years.

# Contents

# List of Figures

# List of Tables

# List of Abbreviations

**AC** alternating current

**BP** Battery package

**DC** direct current

**DL** Dump load

**EC** Effect curve

**HRES** Hybrid renewable energy system

**KVT** Kjeller Vindteknikk

**LOLP** Loss of load probability

**NO** Nordlysobservatoriet

**NOCT** Nominal operating cell temperature

**PL** Primary load

**SPV** Solar photovoltaic

**STC** Standard test conditions

**UiT** UiT the Arctic University of Norway

**WT** Wind turbine

# 1

# Introduction

At Nordlysobservatoriet (NO), Alta there is planned to be installed a weather station. But there is no grid connection in the area, as NO is located on a mountain top 904 m above sea level. Therefor a Hybrid renewable energy system (HRES) is also planned to be installed. The main reason to install the HRES is to provide as a power supply for the weather station. The HRES will consist of two Wind turbine (WT), four Solar photovoltaic (SPV) panels, and a Battery package (BP). This thesis will investigate the HRES performance with respect to power supply to the wather station, or if there needs to be changes to the HRES. Kjeller Vindteknikk (KVT) have been given the mission to install the system, on behalf of UiT the Arctic University of Norway (UiT). A meeting between the two parts have already laid a plan for how the HRES will be set up. This thesis will evaluate this solution, and if there are other options thet could be used to increase power production, or make the system a more reliable power sypply for the weather station.

HRES have previously been used with success arctic regions. In Imnavait Creek, Alaska, a similar energy system was set up to supply a weather station[11]. They experienced that the HRES supplied enough energy to the instruments at all times. The same was the case at Camp Raven on Greenland, just below the arctic circle[6]. On Camp Raven they could rely on the HRES as the only energy resource for three years straight. In both cases wind and solar energy was used as power supply. A combination of both wind and solar energy in a HRES would be more reliable, than just using one of the sources, as there have been studies that suggest that wind and solar power can be complementary in

high-latitude arctic areas[22].

MATLAB® was used to simulate different scenarios for the HRES. The different scenarios used the components agreed on between UiT and KVT, in different set ups, to see how mounting of SPV panels and other factors affected the operation of the system.

# 2

# Theory

## 2.1 Energy resources

### 2.1.1 Wind energy

The power (P) in wind, is the kinetic energy in moving air. Air that that goes through a cross sectional area A, with a density $\rho$, with a velocity v, have a power given as equation 2.1.

$$P = \frac{1}{2} A \rho_{air} v^3 \tag{2.1}$$

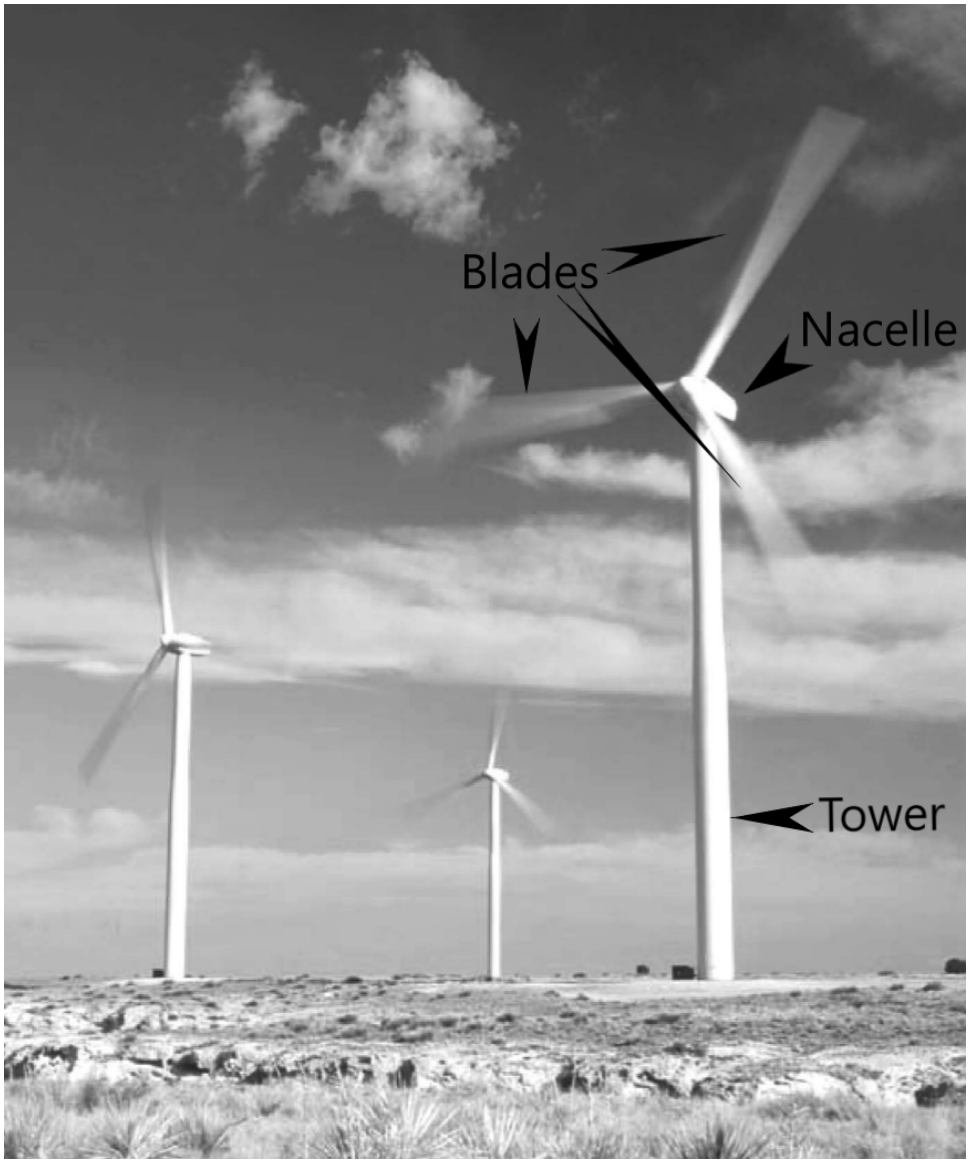


**Figure 2.1:** Three horizontal axis wind turbines[23].

The kinetic power in air can be transformed into electrical power through a wind turbine (WT). Three horizontal axis wind turbines are depicted in figure 2.1. The figure depicts three common hallmarks of a WT. The tower raises the nacelle to a desired height. The nacelle houses a generator that produces electricity. The generation of electricity is driven by a fourth hallmark, the rotor, that is attached to the generator and the nacelle. And the blades are in turn attached to the rotor. In this way, as wind blows onto the blades, the kinetic energy in the air is transformed into kinetic rotational energy. The rotational energy is then again transformed to electric energy in the generator. As such the power production from a WT can be estimated from equation 2.1. But the maximum theoretical efficiency of a WT, called Betz limit, is stated to be $C_{Betz} = 16/27 = 59.3\%$[23]. The theoretical maximum power is given in equation 2.2.

$$P = C_{Betz}\frac{1}{2}A\rho v^3 \tag{2.2}$$

As the wind speed is cubed in equation 2.2, this is the most important variable for electricity production. KVT have provided data series on several variables, including wind speed and wind direction. The data is originally from ERA-Interim, and then KVT have done further work on the data, to get a geographical resolution of 4km.

### 2.1.2 Solar energy

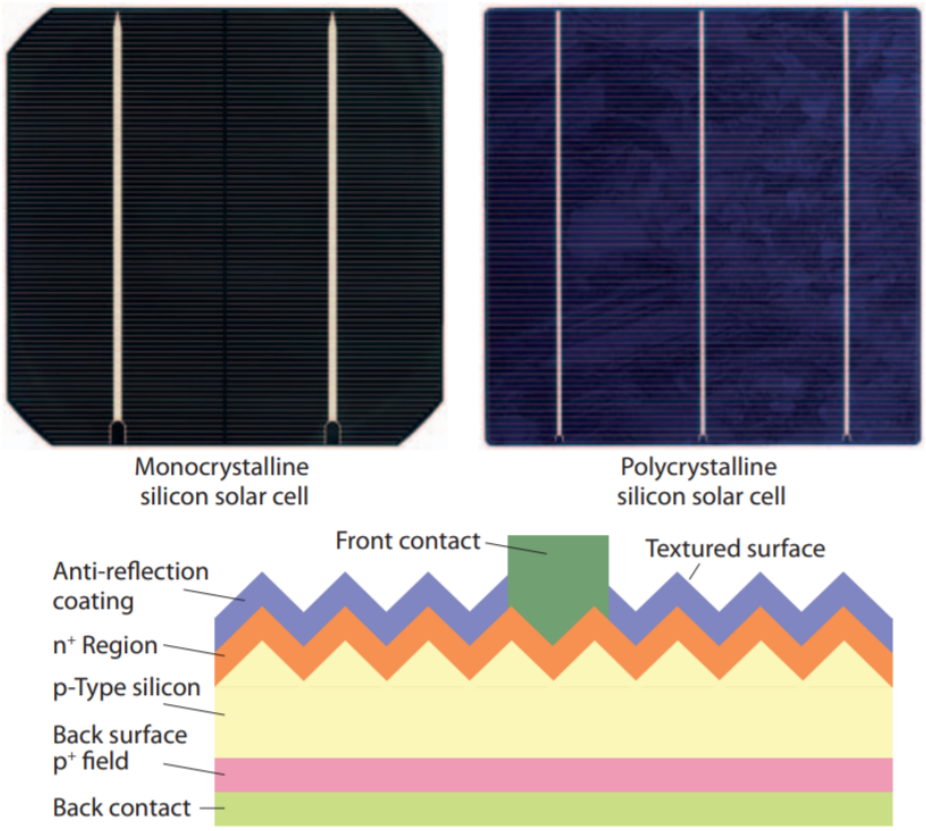


**Figure 2.2:** Typical mono- and poly-crystalline cilicon cells as seen from above (upper two cells), and the layers they are built up by as seen from cross-section from side (lower)[20].

To convert solar radiation power into electric power, SPV panels are used. More than 90% of produced solar cells are of crystalline silicon[21]. Figure 2.2 shows a simplified figure of how a typical silicon solar cells are layered. Between the $n^+$ region, and the p-type silicon, there is a built in voltage potential. As solar radiation shines on the solar cell, electrons in the silicon crystalls absorb the energy in the radiation. This in turn can excite the electrons from their bound state in the silicon stucture, so that they can travel freely. The built in potential will then create a current from the p-type side to the n-type side. If an electrical deivce is coupled to the front and back contacts of the cell, then the current will power the device [21].

There is a Standard test conditions (STC) used on SPV cells to determine the characteristics of the cell. The STC are a radiance of $1000 W/m^2$, a cell temperature of $25^o C$, and an air mass corresponding to 1.5 times the thickness

of the atmosphere (AM1.5). As a cell temperature is typicaly higher than $25^oC$ in operating conditions, there is another concept that shows how the cell temperature will be, called Nominal operating cell temperature (NOCT). The NOCT is defined at a radiance of $800W/m^2$, an ambient temperature ($T_a$) of $20^oC$, and a wind speed of $1m/s$, with the cell mounted with an open back side[21].

Solar radiation data was gathered online from PVGIS (c) European Communities[18].

## 2.2 Devices to be installed

The components to be installed was agreed on between the University of Tromsø (UiT), by the departmend for building and property (BEA), and Kjeller Vindteknikk (KVT), who will deliver the system. The system can be divided into two groups, the power supply and the primary load. The power supply is a HRES. The HRES agreed on consist of two wind turbines, four solar photovoltaic (PV) panels, and a battery package. The main load for the system are measuring instruments. The measuring instruments one pyranometer, three different wind speed measuring devices, one device to measure wind direction, a thermometer, and a hygrometer.

### 2.2.1 HRES components

#### Wind turbine

The wind turbines proposed were the Rutland FM1803-2 Furlmatic Windcharger, coupled with a 24V MPC controller. Figure 2.3 shows the Effect curve (EC) of the WT, as provided from the manufacturer [15]. The figure also depicts a maximum power production of about 850 Watts peak ($W_p$), as also listed in table 2.1. Two such turbines was to be installed, for a total of 1.7k$W_p$ of wind power. Some other characteristics of the WT are listed in table 2.1. It has a cut-in speed of $3m/s$, that is to say it needs a minimum wind speed of $3m/s$ to produce power. While the cut-out speed of $15m/s$ is a safety mechanism, that pushes the turbine from the wind to protect it from high forces.

**Table 2.1:** WT characteristics

| Characteristics | Unit | Value |
|---|---|---|
| Peak power | $W_p$ | 850 |
| Cut-in speed | m/s | 3 |
| Cut-out speed | m/s | 15 |
| Rotor diameter | m | 1.8 |

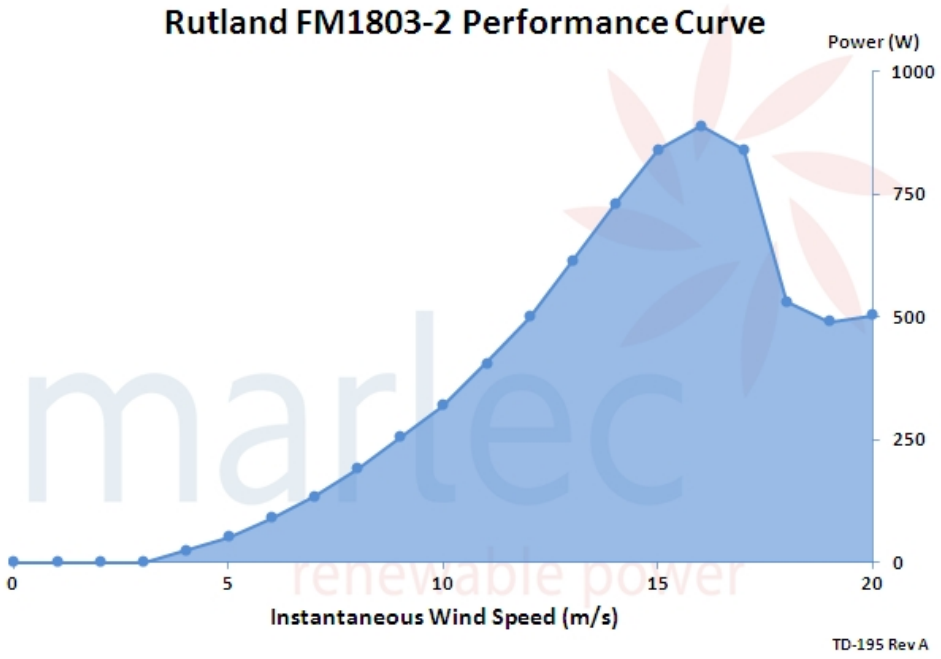


**Figure 2.3:** Effect curve for the wind turbines, as published by manufacturer Marlec[15].

### Solar photovoltaic panel

To utilize solar power, four poly-crystalline silicon SPV panels from Perlight, wired in series, was proposed. With $260W_p$ per panel, the total SPV power to be installed was $1040W_p$. The data sheet for Perlight PLM-270P-60, at $260W_p$ was used as reference for this thesis[17]. To maximize the output power from the SPV panels, the Tristar 30A MPPT (maximum power point tracker) controller was also included to the HRES.

**Table 2.2:** PV panel characteristics [17]

| **Characteristics** | **Short name** | **Unit** | **Value** |
|---|---|---|---|
| Maximum power output | $P_{max}$ | $W_p$ | 260 |
| Voltage at $P_{max}$ | $V_{mpp}$ | V | 30.27 |
| Current at $P_{max}$ | $I_{mpp}$ | A | 8.59 |
| Open-circuit voltage | $V_{OC}$ | V | 36.78 |
| Short-circuit current | $I_{SC}$ | A | 9.15 |
| Module efficiency | $\eta_{ref}$ | % | 15.98 |
| Nominal operating cell temperature | NOCT | $^oC$ | 45 ± 2 |
| Temperature coefficient of $P_{max}$ | $\beta$ | $\%/^oC$ | −0.40 |
| Module dimensions (L W H) | | mm | $1640x992x35$ |
| Panel area | $A_{SPV}$ | $m^2$ | 1.6269 |

Table 2.2 includes some of the characteristivs of the SPV panels. One to note is the tempterature coefficient, $\beta$, that shows how the efficiency of the panels are affected by temperature. As $\beta$ is negative constant, the efficiency of the panels increases linearly with decreasing temperature. Figure 2.4 indirectly shows that the efficiency also depends on the solar radiation intensity. As the different intensity levels induces different SPV efficiencies, the points can be used to estimate the effect of intensity on the SPV efficiency, $\eta_{ref}$.

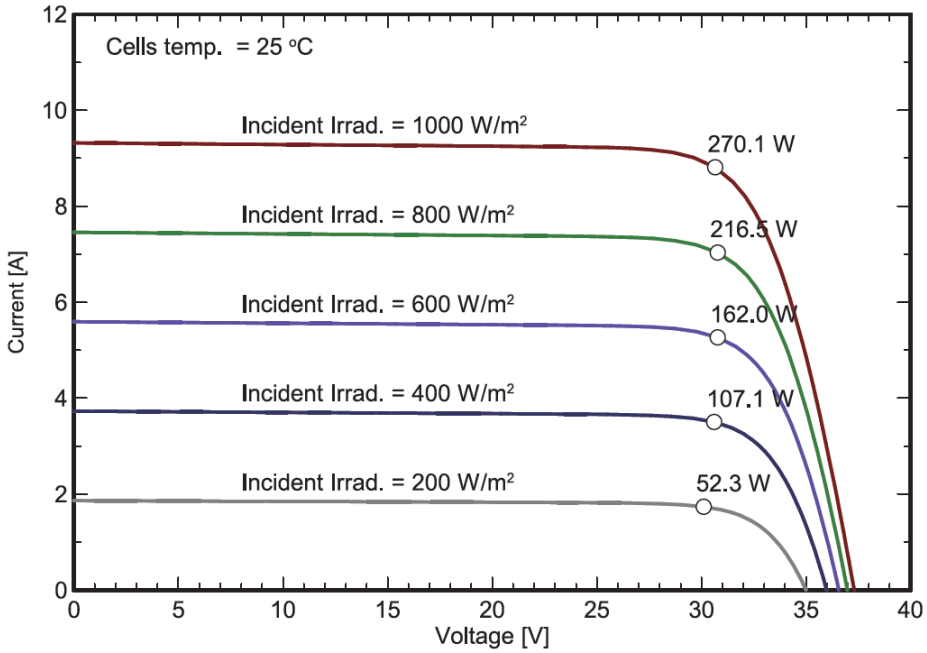


**Figure 2.4:** Solar radiation intensity effect on production by the SPV panel[17].

### Battery package

The battery proposed to the HRES, was the HZY $200Ah - 12V$ sealed deep cycle gel battery. 8 such batteries was to be wired in series and parallel to get $24VDC$. That equates to a BP of $800Ah$, with $24VDC$, as there will be two series in parallel, with four batteries in each of the series. In terms of energy that will be a maximum capacity for the BP as given in equation 2.3.

$$E_{B,max} = 800Ah \cdot 24V = 19.2kWh \tag{2.3}$$

The data sheet for Haze HZY - GEL batteries state the dimension of one HZY $200Ah - 12V$ battery to be 522mm in length, 240mm in width, and 220mm in height. And one such battery will weigh 63.0kg[14]. With eight batteries, that adds up to 504kg for the BP.

## 2.2.2 Measuring devices

The Primary load (PL) for the HRES is a weather station, to measure different variables such as wind speed and direction, solar radiation, humidity and temperature. The different devices that was proposed to be installed are described below, together with an analysis of their power needs.

### Wind measuring devices

To measure wind speed, it was agreed to install three different anemometers. Two cup anemometers, one with, and one without heating. The third device to measure wind speed was an ultrasonic wind sensor from Gill windsonic with heating. A fourth device was agreed to measure the wind direction.

The cup anemometer without heating was the Thies First Class windsensor [5]. The user manual for the product states that the power supply needs to deliver a voltage in the range of 3.7 – 42V DC, with a typical current of 40mA up to a maximum of 100mA. This results in a maximum power need of $42V \cdot 100mA = 420mW = 0.42W$.

The cup anemometer with heating was the Vaisala Anemometer[25]. The power supply needs to deliver a voltage in the range of 9.5 – 15.5 VDC, and a typical current of 20mA. That results in a typical power need of $12V \cdot 20mA = 240mW = 0.24W$ for the device to operate. The heater for the anemometer is

stated to need 20 VDC or VAC, at typical 500mA. Resulting in power need of $20V \cdot 500mA = 10W$.

The NRG 200P Wind Vane, from NRG Systems, was proposed to measure wind direction. The device works such that the vane naturally points itself in the direction of the wind. A potensiometer is coupled to the vane, and as such will point in the same direction as the vane. The potensiometer has a size of $10k\Omega$, and uses a power supply of 15 V DC. That results in a power use of $\frac{(15V)^2}{10k\Omega} = 22.5mW = 0.0225W$ [24].

The Ultrasonic windsensor, WindSonic M, from Gill Instruments requires a DC power supply, with voltages in the range of $5 - 30$ V DC. Typical current drain is 5.5mA at 12V results in power need of $66mW = 0.066W$. But the heater for the Windsonic M is the largest power drain of all the devices. the heater uses a voltage in the range of $10 - 30$ V DC, and can be allowed for a nominal supply of maximum 100W with a current of 4.2A at 24V[12].

### Solar radiation measuring device

The pyranometer that was proposed to measure the solar radiation, was the $SP - 510 - SS - 10$ Thermophile pyranometer [3]. The device itself does not use an external power supply, as it is self-powered. However, the device comes with a heater. The heater draws a $15.4mA$ current at a voltage of $12V$ DC, resulting in a power requirement of $185mW$.

### Other devices

In addition to the wind- and solar-measuring instruments, a thermometer and a hygrometer is part of the weather station. Thermometers and hygrometers usually have low power needs to operate. And since there where no spesifications on the devices to be used, it's asumed in this thesis that they need less than 10W to operate.

In conclusion the wind- and solar-measuring instruments needs less than 11W to operate (without heating), as estimated by above values. Other devices that need some power is the Tristar 30A MPPT controller, as well as communication devices for transmitting the collected data. The largest power needs are for the heaters on the devices equipped with them. In particular the Windsonic M sensor that can draw up to 100W.

## 2.3 Modeling of hybrid renewable energy system

MATLAB® was used to model the system, and it was assumed that the HRES would operate 24h a day, and therefore equipment breakdowns, planned maintenance and so on, were not considered.

### 2.3.1 Wind turbine

To model a WT, there is a common used method that divides the production from wind into three or four wind speed levels. The first level goes from no wind, and up to a chosen cut-in wind speed. For this level there is no production, $0W$ between $v = 0m/s$ and $v = v_{cut-in}$. The second level goes from the cut-in wind speed, to the rated wind speed. The production in this level normally follows equation 2.2, with an additional factor for the typical efficiency of WTs. The rated speed is the wind speed where the WT has it's production peak. The third level then goes from the rated wind speed, to the cut-out wind speed. In this level the production is often set to a constant rated power. The fourth level is after the cut-out wind speed, where the production is set to zero. The third and fourth levels can be combined so that the rated wind speed is equal to the cut-out wind speed[7] [1] [9]. But since the EC of the featured WT was given from the manufacturer in figure 2.3, this was used instead. Figure 2.5 shows the EC together with the efficiency of the turbine at different wind speeds. The efficiency of the turbine was calculated by dividing the output power from the turbine, on the power in the wind.

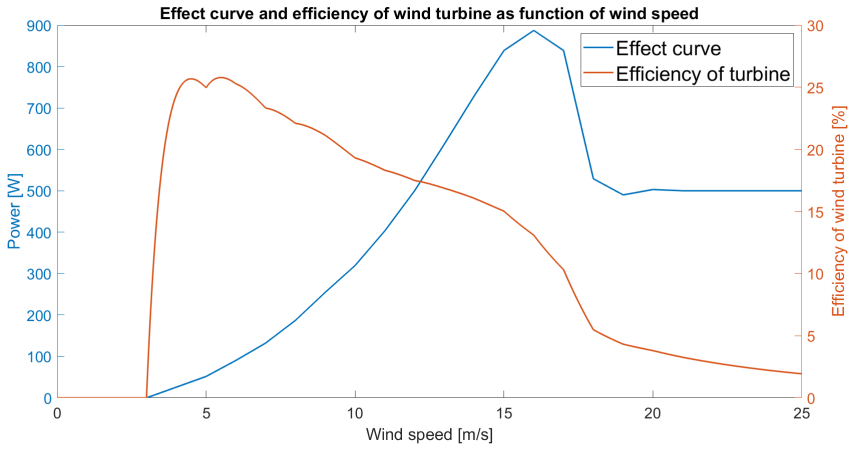


**Figure 2.5:** Effect curve for the wind turbines, from manufacturer. As well as the efficiency of the wind turbines, as power produced divided on power in the wind at each given wind speed.

### 2.3.2 Solar photovoltaic panels

To estimate the power production from SPV, the simplest method is to multiply incoming radiation $I_{panel}(t)$ with the given efficiency of the SPV panels, and also taking the panels area into account[10]. But there are other variables and conditions that have an impact on the efficiency and output power of the panels. $\eta_{pc}$ is the power conditioning efficiency. $\eta_{pc}$ is equal to 0.9 with a perfect maximum point tracker [1][13]. Consider the tristar 30A MPPT as perfect in the simulations. Increasing temperature have a negative effect on the efficiency of a SPV panel. Equation 2.4 shows energy conversion from radiation to electricity, with the temperature dependency of $\eta_{ref}$[4][8].

$$E_{SPV} = \cdot I_{panel}(t) \cdot A_{SPV} \cdot \eta_{ref} \cdot \eta_{pc} \cdot \left(1 - \beta \cdot \left(T_a(t) - T_{ref} + (T_{NOCT} - T_{a,NOCT}) \cdot \frac{I_{panel}(t)}{I_{NOCT}}\right)\right) \quad (2.4)$$

$\beta$ is the temperature coefficient of the panel, given in table 2.2 as $-0.4\%/^oC$. The different temperatures are the ambient temperature $T_a(t)$, the cell temperature at STC $T_{ref} = 25^oC$, the NOCT $T_{NOCT} = 45^oC$, and the ambient temperature at NOCT $T_{a,NOCT} = 20^oC$. $I_{NOCT}$ is the intensity used at NOCT equal to $800W/m^2$.

In this thesis the intensity effect on $\eta_{ref}$ was also taken into consideration. Equation 2.5 shows the full modell for the SPV panels used in the simulations.

$$E_{SPV} = \cdot I_{panel}(t) \cdot A_{SPV} \cdot \eta_{ref} \cdot \eta_{pc} \cdot \left(1 - \beta \cdot \left(T_a(t) - T_{ref} + (T_{NOCT} - T_{a,NOCT}) \cdot \frac{I_{panel}(t)}{I_{NOCT}}\right)\right) \cdot \left[\left(k_1 + k_2 I_{panel}(t) + k_3 I_{panel}^2(t) + k_4 I_{panel}^3(t) + k_5 I_{panel}^4(t)\right) - \eta_{diff}\right] \cdot \frac{1}{\eta_{ref}} \quad (2.5)$$

The intensity factor in equation 2.5 is a relative effect, as shown in figure 2.6. The intensity effect is actually a logarithmic factor of the radiation intensity [16][19]. But in this thesis it's mathematically adapted as a polynom, to the intensity points that was shown in figure 2.4. These points are summed up in table 2.3, and also plotted as an relative effect alongside the estimated factor in

figure 2.6. The efficiencies in table 2.3 were calculated as the SPV panel output, divided on the area of the panel, and on the intensity at the corresponding output, for example $\eta_{200} = 52.3/(A_{SPV} \cdot I_{200})$. Since the points were from a solar panel manufactured with a slightly higher efficiency than the one used in this thesis, the factor was corrected by subtracting the difference of the two efficiencies, $\eta_{diff} = 0.62\%$.

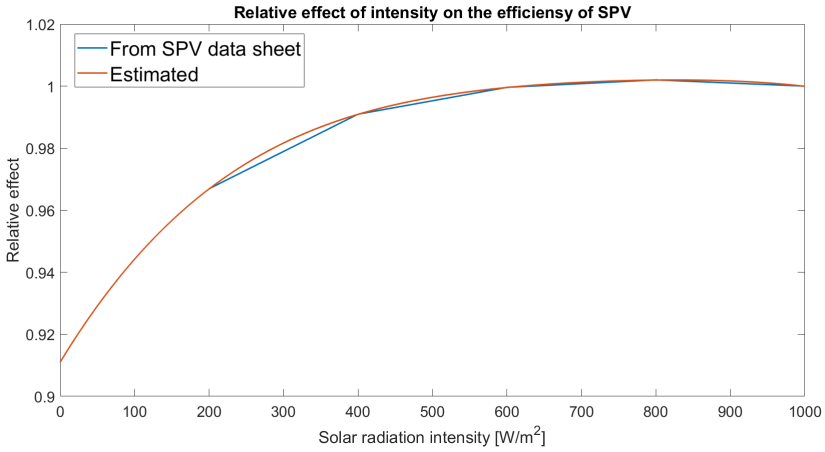


**Figure 2.6:** Estimated relative effect of solar radiation intensity on the efficiency of SPV panels, together with effect from Perlight data sheet.

**Table 2.3:** Efficiency for the different solar irradiation intensities, as shown in figure 2.4.

| **Incident irradiation** $[W/m^2]$ | **SPV panel output** $[W]$ | **Efficiency at given intensity** [%] |
|---|---|---|
| $I_{200} = 200$ | 52.3 | $\eta_{200} = 16.07$ |
| $I_{400} = 400$ | 107.1 | $\eta_{400} = 16.45$ |
| $I_{600} = 600$ | 162.0 | $\eta_{600} = 16.60$ |
| $I_{800} = 800$ | 216.5 | $\eta_{800} = 16.63$ |
| $I_{1000} = 1000$ | 270.1 | $\eta_{1000} = 16.60$ |

The coefficients $k_1, .., k_5$ in the polynom in equation 2.5, were found by solving the equations 2.6-2.10. To make the calculations easier, the equations were set up in matrix form, as in equation 2.11.

$$k_1 + k_2 \cdot I_{200} \quad +k_3 \cdot I_{200}^2 + k_4 \cdot I_{200}^3 \quad +k_5 \cdot I_{200}^4 = \eta_{200} \tag{2.6}$$
$$k_1 + k_2 \cdot I_{400} \quad +k_3 \cdot I_{400}^2 + k_4 \cdot I_{400}^3 \quad +k_5 \cdot I_{400}^4 = \eta_{400} \tag{2.7}$$
$$k_1 + k_2 \cdot I_{600} \quad +k_3 \cdot I_{600}^2 + k_4 \cdot I_{600}^3 \quad +k_5 \cdot I_{600}^4 = \eta_{600} \tag{2.8}$$
$$k_1 + k_2 \cdot I_{800} \quad +k_3 \cdot I_{800}^2 + k_4 \cdot I_{800}^3 \quad +k_5 \cdot I_{800}^4 = \eta_{800} \tag{2.9}$$
$$k_1 + k_2 \cdot I_{1000} \quad +k_3 \cdot I_{1000}^2 + k_4 \cdot I_{1000}^3 \quad +k_5 \cdot I_{1000}^4 = \eta_{1000} \tag{2.10}$$

Matrix form
$\Downarrow$

$$\begin{bmatrix} 1 & I_{200} & I_{200}^2 & I_{200}^3 & I_{200}^4 \\ 1 & I_{400} & I_{400}^2 & I_{400}^3 & I_{400}^4 \\ 1 & I_{600} & I_{600}^2 & I_{600}^3 & I_{600}^4 \\ 1 & I_{800} & I_{800}^2 & I_{800}^3 & I_{800}^4 \\ 1 & I_{1000} & I_{1000}^2 & I_{1000}^3 & I_{1000}^4 \end{bmatrix} \begin{bmatrix} k_1 \\ k_2 \\ k_3 \\ k_4 \\ k_5 \end{bmatrix} = \begin{bmatrix} \eta_{200} \\ \eta_{400} \\ \eta_{600} \\ \eta_{800} \\ \eta_{1000} \end{bmatrix} \tag{2.11}$$

The different matrices were given the names $I_{intensity}$, $K$, and $\eta_{intensity}$, as shown in equation 2.12.

$$I_{Intensity} = \begin{bmatrix} 1 & I_{200} & I_{200}^2 & I_{200}^3 & I_{200}^4 \\ 1 & I_{400} & I_{400}^2 & I_{400}^3 & I_{400}^4 \\ 1 & I_{600} & I_{600}^2 & I_{600}^3 & I_{600}^4 \\ 1 & I_{800} & I_{800}^2 & I_{800}^3 & I_{800}^4 \\ 1 & I_{1000} & I_{1000}^2 & I_{1000}^3 & I_{1000}^4 \end{bmatrix}, K = \begin{bmatrix} k_1 \\ k_2 \\ k_3 \\ k_4 \\ k_5 \end{bmatrix}, \eta_{intensity} = \begin{bmatrix} \eta_{200} \\ \eta_{400} \\ \eta_{600} \\ \eta_{800} \\ \eta_{1000} \end{bmatrix} \tag{2.12}$$

By multiplying the inverse of $I_{intensity}$, on both sides in equation 2.11, the coefficient matrix K could be isolated. As shown in equations 2.13-2.15.

$$I_{intensity} \cdot K = \eta_{intensity} \tag{2.13}$$
$$\rightarrow \quad I_{intensity}^{-1} \cdot I_{intensity} \cdot K = I_{intensity}^{-1} \cdot \eta_{intensity} \tag{2.14}$$
$$\rightarrow \quad K = I_{intensity}^{-1} \cdot \eta_{intensity} \tag{2.15}$$

With K isolated, the values from table 2.3 was set into the matrices $I_{intensity}$ and $\eta_{intensity}$. The coefficients in K was then calculated by matrix multiplication, and are given in equation 2.16.

$$K = \begin{bmatrix} k_1 \\ k_2 \\ k_3 \\ k_4 \\ k_5 \end{bmatrix} = \begin{bmatrix} 0.1518 \\ 6.319611772 \cdot 10^{-5} \\ -1.09808857 \cdot 10^{-7} \\ 9.12405955 \cdot 10^{-11} \\ -3.041353183 \cdot 10^{-14} \end{bmatrix} \tag{2.16}$$

As the points from the SPV data sheet was for intensities between $200W/m^2$ and $1000W/m^2$, this would also be the valid interval for the intensity factor. But it was assumed that the estimated intensity factor could be used for the interval between $0W/m^2$ and $1000W/m^2$ in the simulations.

### 2.3.3 Load profile

The PL was modeled as function of temperature, where the load was set to different constants at different temperature levels. There where also done simulations with a high PL constant = $150W$. At constant PL= $150W$, the HRES would need to at least produce $150W \cdot 8760h/year = 1314kWh$, to have any chance of meeting the PL. The temperature levels was set as equation 2.17.

$$P_{PL}(T(t)) = \begin{cases} 20W, & T > 0^oC \\ 75W, & 0^oC \geq T > -10^oC \\ 100W, & -10^oC \geq T > -20^oC \\ 150W, & T \leq -20^oC \end{cases} \tag{2.17}$$

### 2.3.4 Battery storage

Modeling of the battery capacity, $E_b$ at time t was set as equation 2.18 [13].

$$\begin{aligned} E_b(t) =& E_b(t - \Delta t) \\ &+ (E_{WT}(t) + E_{SPV}(t)) \cdot \eta_{cha} \cdot \eta_{inv} \cdot \eta_{wr} - \frac{E_{PL}(t)}{\eta_{inv}\eta_{wr}} \end{aligned} \tag{2.18}$$

with the constraint that;

$$0 \leq E_b \leq E_{b,max} \tag{2.19}$$

The HRES also included a low voltage disconect module, to stop the supply if the voltage of the BP droppes to low, but in the modell of the system it is assumed that the battery can be drained of all charge. As the self-discharge rate of the battery is only 0.005% per hour, it is assumed to be zero [26]. Charge efficiency $\eta_{cha}$ was set to 0.95% [26]. The different connections in the HRES that goes from alternating current (AC) to direct current (DC) (AC/DC), or just a transformation of DC voltage (DC/DC) needs an inverter. The invertion efficiency, $\eta_{inv}$, was assumed to be 95% [1]. If the battery was at full capacity, and the HRES produced more power than demanded by the PL, the excess power was delivered to a Dump load (DL).

### 2.3.5 Loss of load probability

Loss of load probability (LOLP) depicts how much time the power demand of the PL exceeded the supply from HRES. The formula is given in equation 2.20 [26].

$$LOLP = \frac{\sum_{t=1}^{n} hours(E_{supply}(t) < E_{demand}(t))}{n} \tag{2.20}$$

Where n is the total number of hours simulated over, $E_{supply}(t)$ is available energy to be used at time t, and $E_{demand}(t)$ is the energy needed for the PL at time t.

# /3 Halddetoppen

**Figure 3.1:** Nordlysobservatoriet at Halddetoppen, Alta.[Picture taken by author of thesis]

Halddetoppen is a mountain top about 13.5km from Alta town, Finnmark. On the mountain top there are two larger buildings. One of those are Nordlysobservatoriet (NO), which is in the picture of figure 3.1. Halddetoppen is located at a latitude $\phi = 69.939^o$ north, and at a longditude $\lambda = 22.923^o$ east. NO lies at 904 meters above sea level. As top is so high, there are few obstacles that in any way can shade for the NO. That is probably one of the reasons why the norwegian scientist Kristian Birkeland, in his day founded NO to study the aurora borealis. NO is not longer used for astronomic research, but is used by UiT and Alta og omegn turlag, for more recreational purposes.

Now a HRES will be installed at the place, in first place to work as a power supply for a weather station. Four SPV panels are planned to be mounted on the tower in figure 3.1. As the picture shows, there already is installed a small SPV panel on the south-west wall. Two more panels will be installed on that wall, with the other two on the south-east wall in the middle of the picture. Two WTs will be mounted on a mast to the left behind the picture. And a BP will be placed inside the building.

As Halddetoppen is above the arctic circle, the sun is below the horizon for a considerable period of the year. The sun is below the horizon from Novemver $25^{th}$, until January $17^{th}$ in Alta.

# 4

# Method

## 4.1 Weather data

Data on the variables wind speed, wind direction, solar radiation, temperature, and pressure, were provided by KVT. But as the solar radiation values was given on a horizontal surface, it proved difficult to redirect the beam onto the panels, as some small angle factors would blow up the apparent radiation. The solar data provided was also the global radiation, so consisted of both direct beam radiation, and diffuse radiation. Since the diffuse radiation isn't homogeneously distributed over the sky, it would be difficult to separate the diffuse and direct fractions from the data. Therefore, solar radiation data was downloaded from PVGIS (c) European Communities[18]. PVGIS uses data from ERA5 to modell solar radiation. Data series from KVT started in 1979 and consisted of all years up to and including 2018. The data from PVGIS on the other hand was only from the years 2010 – 2016. Both data sets, and all data series, was on an hourly basis, which is sufficient to get a good estimation of wind and solar power[2]. As the data from KVT was on a 4km grid, the closest grid point to Halddetoppen was 1541 meters away from the station. The height above sea level at this point in the grid, was 569.7 meters, which is lower than Halddetoppen. Data from PVGIS is on grid of about 30km, same as the ERA5 data.

### 4.1.1 Wind data

The wind data from KVT was given for different heights above the surface, and one at 10 meters height was chosen, as this was the height the WT were planned to have. Figure 4.1 shows the average hourly wind speed from 2010 that were used in the simulations.

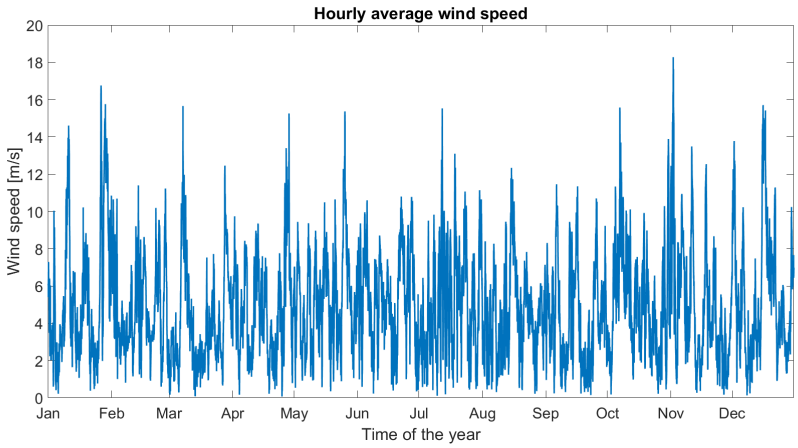


**Figure 4.1:** Hourly average wind speed at Halddetoppen as modelled by KVT in 2010.

In figure 4.2 and 4.3 wind roses from the year 2010 and the years 1980-2017, respectively, are shown. They show that the wind directions are fairly constant over longer periods.

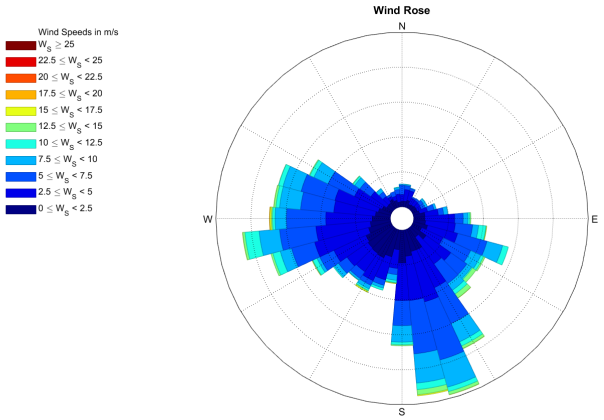


**Figure 4.2:** Wind direction at Halddetoppen as modelled by KVT 2010.

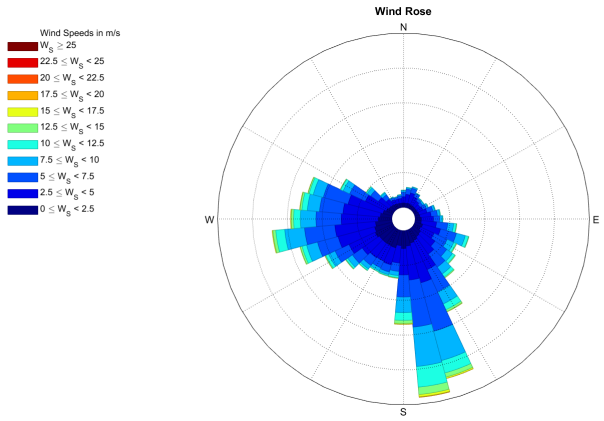


**Figure 4.3:** Wind direction at Halddetoppen as modelled by KVT 1980-2017.

Figure 4.4 and 4.5 shows the distibutions of wind speeds in the year 2010 and the years 1980-2017, respectively. A weibull distribution fitted to the years 1980-2017, is displayed in both figures. The figures show that it blew somewhat weaker in 2010 than in other years from the data set. This is also supported by table 4.1, that shows the average wind speeds from the years 2010-2017, as well as the average wind speed for all the years 1980-2017.

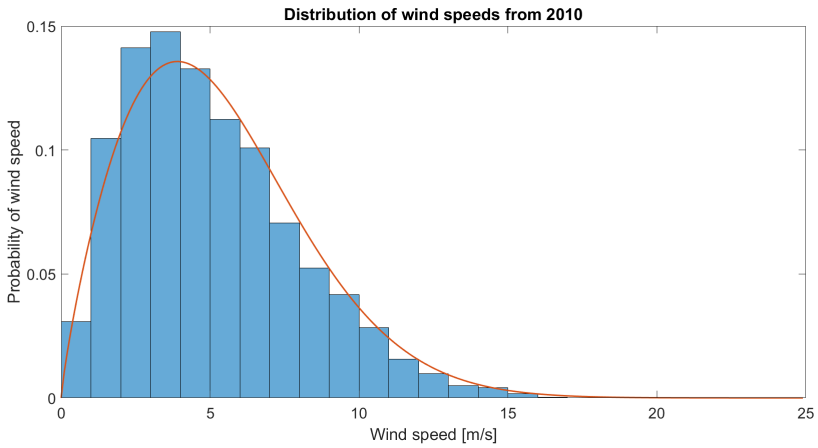


**Figure 4.4:** Distribution of windspeeds from modelled data in 2010.

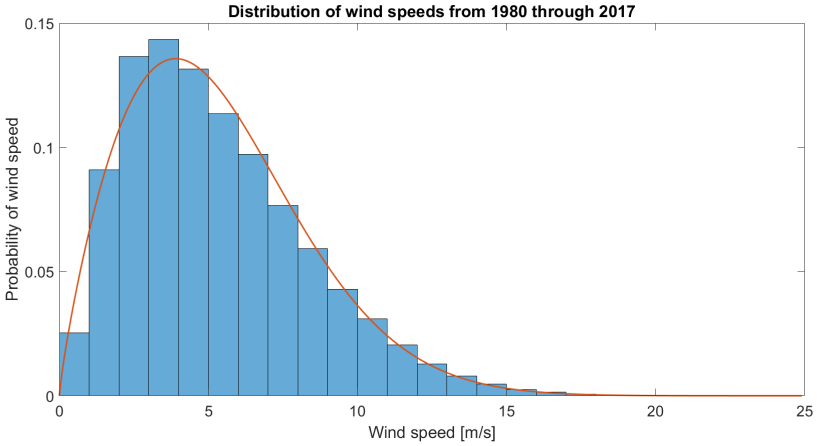


**Figure 4.5:** Distribution of windspeeds from modelled data 1980-2017.

**Table 4.1:** Average wind speeds for each of the years 2010-2016. Also average wind speed for all data points between 1980-2017.

| Year | Unit | Average wind speed |
|---|---|---|
| 2010 | $m/s$ | 4.89 |
| 2011 | $m/s$ | 5.55 |
| 2012 | $m/s$ | 5.31 |
| 2013 | $m/s$ | 5.09 |
| 2014 | $m/s$ | 5.15 |
| 2015 | $m/s$ | 5.71 |
| 2016 | $m/s$ | 5.04 |
| 1980-2017 | $m/s$ | 5.31 |

### 4.1.2 Solar data

Solar data from PVGIS was downloaded from their website[18], where several parameters was used as input to get the correct data. The latitude and longditude of Halddetoppen, $\phi = 69.939^o$north and $\lambda = 22.923^o$east respectively, was used to set the location. The placement of the SPV panels also had angle inputs. As the plan was to mount them on the south-west and south-east walls of NO two data set was downloaded. One set with an azimuth angle of $45^o$, corresponding to south-west, and one with azimuth angle of $-45^o$, corresponding to south-east. Both sets with a slope of $90^o$, as they would be standing on the wall. The solar radiation was divided into in-plane beam irradiance, in-plane diffuse irradiace, and in-plane reflected irradiance. It was not stated if the in-plane reflected irradiance was calculated with reflections from snow taken into account. But other parameter from PVGIS was stated to eliminate snow effects, so it was assumed that the reflected irradiance from the data set didn't take reflections from snow into account. All variables were in units of $W/m^2$. Another effect PVGIS took into account, was the horizon height as depicted in figure 4.6. The figure shows a higher horizon to the west than to the east. The figure also depictis the sun height in June and December. But as the sun is below the horison at Halddetoppen through December, the sun height in December was not depicted. Horizon height have an impact on the total irradiance on the two walls, as they are facing to the south-east and south-west, and not directly south, where the horizon height is zero. That is supported by table 4.2 that shows the total irradiance density on each of the walls for all available years, and an average irradiance density for those years. The east wall, with a lower horizon height in front of it gets a higher irradiance density on it.

**Table 4.2:** Total solar insolation on both the south-west and south-east walls for the years 2010-2016.

| **Year** | **Unit** | $I_{south-westwall}$ | $I_{south-eastwall}$ |
|---|---|---|---|
| 2010 | $kWh/m^2$ | 650.5 | 691.0 |
| 2011 | $kWh/m^2$ | 695.3 | 718.6 |
| 2012 | $kWh/m^2$ | 651.2 | 691.6 |
| 2013 | $kWh/m^2$ | 718.0 | 744.0 |
| 2014 | $kWh/m^2$ | 704.1 | 726.0 |
| 2015 | $kWh/m^2$ | 646.8 | 653.5 |
| 2016 | $kWh/m^2$ | 660.4 | 686.3 |
| Average | $kWh/m^2$ | 675.2 | 718.6 |

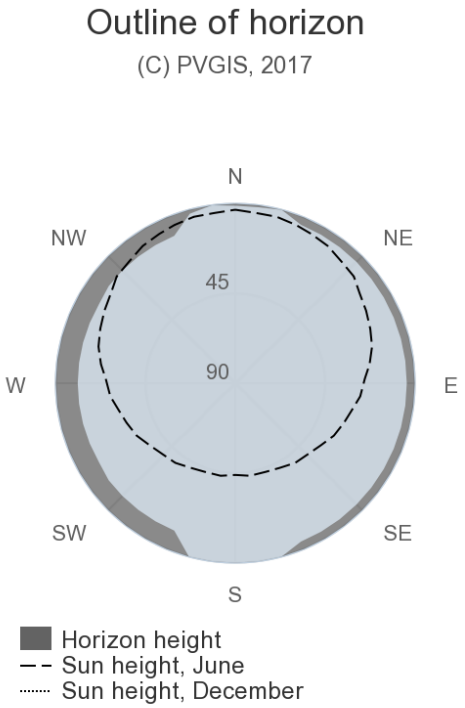


**Figure 4.6:** Horizon height as seen from Halddetoppen[18].

Figures 4.7 and 4.8 shows the irradiance on the south-east and south-west walls, respectively. The data for the figures was from 2010, and this data was used in the simulations.

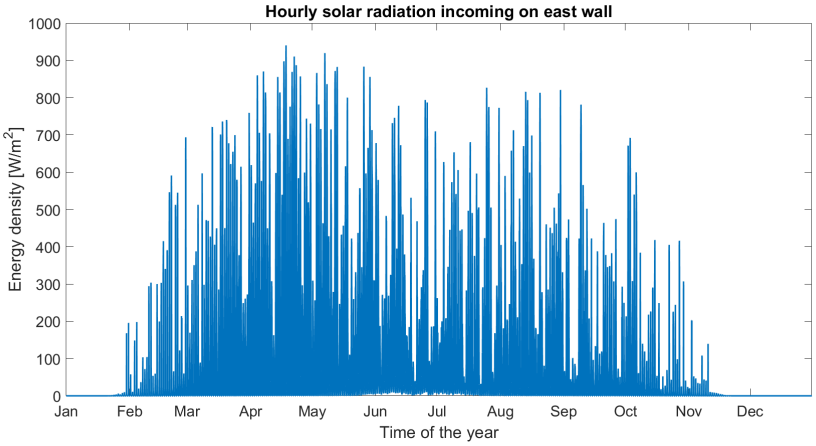


**Figure 4.7:** Solar radiation density on the panels placed on the south-east wall, in 2010.

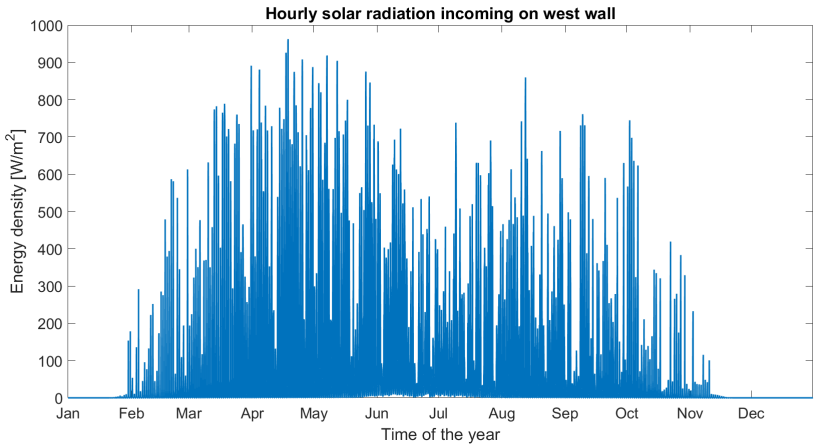


**Figure 4.8:** Solar radiation density on the panels placed on the south-west wall, 2010.

### 4.1.3 Temperature and pressure data

Figures 4.9 and 4.10 shows the ambient tempetature and pressure, respectively, as modelled by KVT from 2010. The temperature data was used both in calculation of SPV production, and to model the PL. The pressure data was not used. But wind power is dependent on air density from equation 2.2. And air density is directly proportional to pressure. As such the pressure of the site will affect wind power production. But as depicted in figure 4.10 the pressure one ATM is of order $10^5$, and as such the relative difference compared to the pressure at Halddetoppen becomes negligible.

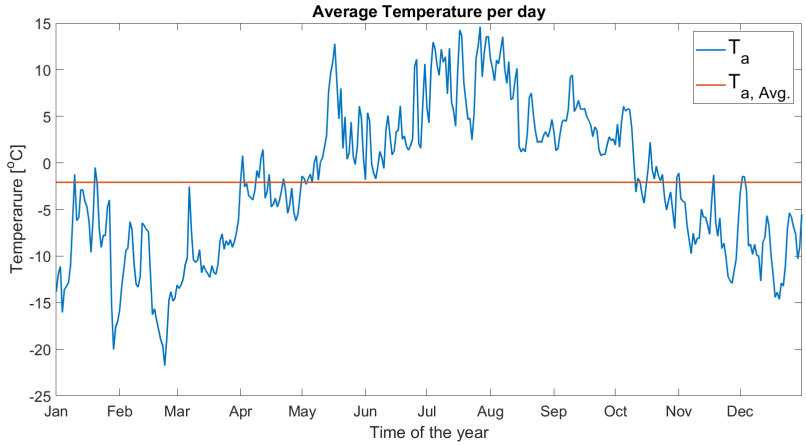


**Figure 4.9:** Temperature at Halddetoppen, with an average temperature of $-2.087^oC$, in 2010.

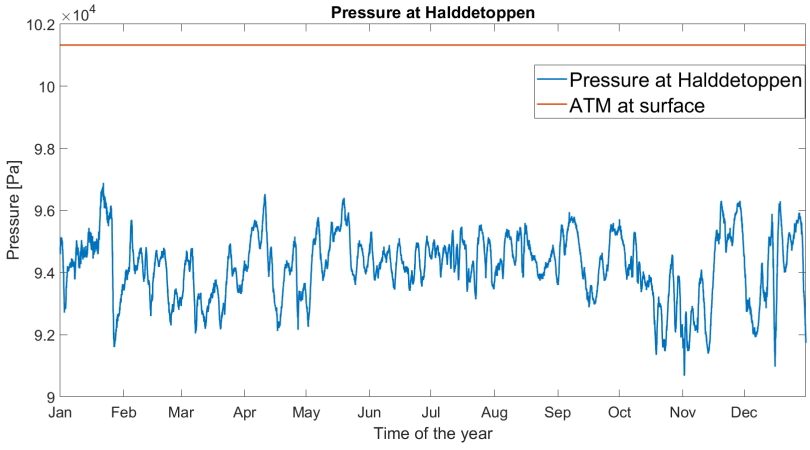


**Figure 4.10:** Pressure at Halddetoppen as modelled by KVT in 2010. Also the constant 1 Atmospheric pressure at surface is displayed.

## 4.2 Simulation set-up

Data from 2010 was used for the simulations, unless otherwise stated. Different scenarios was looked at, to find possible methods to set up the HRES.

### 4.2.1 Planned scenario

In the Planned scenario, senario 1, the HRES was simulated as the set-up that was agreed on between UiT and KVT. In this scenario the two WTs were mounted in a mast below NO, with the nacelles at 10 meters height. They were modelled only with the EC given from the manufacturer, and simulated with wind speed data from 2010 as input. The wind power also depends on, via air density, pressure and temperature. It is direcly proportional with pressure, and inversly proportional with temperature, but these dependencies were not taken into account in the modell. It was further assumed that they don't interfere with each other, and that they will produce the same amount of power.

The SPV panels are modelled after equation 2.5. With two panels on each wall, $I_{panel}(t)$ was set to the irradiance on the two respective walls. It was assumed assumed panels mounted on the same wall would produce the same amount of power.

The BP was modelled after equation 2.18. It was assumed to be at full capacity at the start of each simulation. It was also assumed that it could be drained of all capacity.

The PL was simulated both with a temperature dependent profile, as given in equation 2.17, and with a constant high load demand at $P_{PL} = 150W$.

Key values from the simulations includes;

- Total numbers from energy production.
- Capacity factor for the WTs, calculated as total energy production from wind divided by potential production from wind (that is, theoretical maximum production).
- Capacity factor for the SPV panels, calculated as total energy production from SPV divided by potential production from SPV.
- Energy delivered to both PL and DL.
- Loss of load probability (LOLP) for energy supply to PL

### 4.2.2 Optimal production

For the optimal production scenario, scenario 2, the SPV panels were simulated as mounted in optimal angles (slope and azimuth), compared to the placement on the building walls in scenario 1. In addition to put in values for slope and azimuth angles, the PVGIS tool could be set to compute these angles for optimal production. The angles then became $49^o$ for the slope, and $-5^o$ for the azimuth. So the panels would all be oriented $5^o$ towards the east, from south. In this scenario $I_{panel}(t)$ was the same variable for all panels, and all panels was assumed to produce the same amount of power.

### 4.2.3 All SPV panels on south-east wall

As the horizon to the east had a lower height than to the west, a scenario with all panels on the east wall was simulated, scenario 3. This scenario was very similar to scenario 1, with the only difference that all SPV panels were mounted on the south-east wall, and none on the south-west wall.

### 4.2.4 Only wind turbines

As wind power is potentially available at every moment of the year, a scenario with only WTs was simulated, scenario 4. In this scenario there were no SPV panels, and no solar power involved. This scenario was also simulated with more than one WT, and also with a larger battery capacity. All WTs was mounted in the same way as for the Planned scenario. And it was assumed that all WTs would generate the same amount of energy.

### 4.2.5 Only SPV panels

A scenario with only SPV panels was simulated, scenario 5, to see how large the BP would have to be if SPV was to be the only energy source for the PL. As long as the yearly energy production from SPV was larger than the yearly energy demand of the PL, only the BPs size would keep it from working. In this scenario there was no producion from wind. And the SPV panels was assumed to be mounted two on each wall of NO, as in scenario 1. Instead of simulating from January 2010 until January 2011, it was simulated from July 2010 until July 2011. This was done to cover all of the polar night, when the sun would be below the horizon.

# 5 Results

## 5.1 Planned scenario

The key values from scenario 1 are listed in table 5.1 below. Can see from the table that the HRES manages to supply the PL through the year, as the LOLP= 0, but not for the case of a constant high PL.

**Table 5.1:** Results for system as it was planned, with model data from 2010.

| Parameters | Short name | Unit | Value |
|---|---|---|---|
| Total energy production | $E_{tot}$ | kWh | 2140.4 |
| Energy production from WT | $E_{WT}$ | kWh | 1499.7 |
| Energy production from PV | $E_{PV}$ | kWh | 640.7 |
| Capacity factor for WT | $C_{WT}$ | % | 9.65 |
| Capacity factor for PV | $C_{PV}$ | % | 7.03 |
| Energy delivered to primary load, with variable PL | $E_{PL}(T)$ | kWh | 500.6 |
| Energy delivered to dump load, with variable PL | $E_{DL}(T)$ | kWh | 1453.7 |
| Loss of load probability, PL | LOLP | % | 0 |
| Energy delivered to primary load, with constant PL | $E_{PL,C}$ | kWh | 1239.0 |
| Energy delivered to dump load, with constant PL | $E_{PL,C}$ | kWh | 608.1 |
| Loss of load probability, with constant PL | LOLP | % | 5.71 |

The figures 5.1, 5.2, and 5.3, shows the daily production of the HRES, WTs, and SPV panels, respectively. Can see that daily maximum wind power production, towers the daily maximum production from SPV. The average production per day for the HRES was $E_{tot}$ = 5.86kWh in 2010.

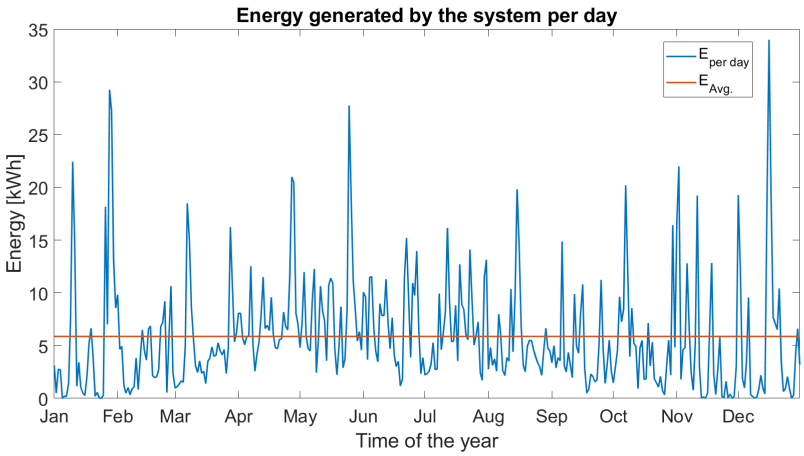


**Figure 5.1:** Estimated production by HRES, along with the average production, both per day, in 2010.

The average production by WTs in 2010 was $E_{WT}$ = 4.11kWh per day. Can see from figure 5.2 that there are large variations from WT production in 2010. 70.7% of the days in 2010, had a production under 5kWh. While some days had over 20kWh of energy production.

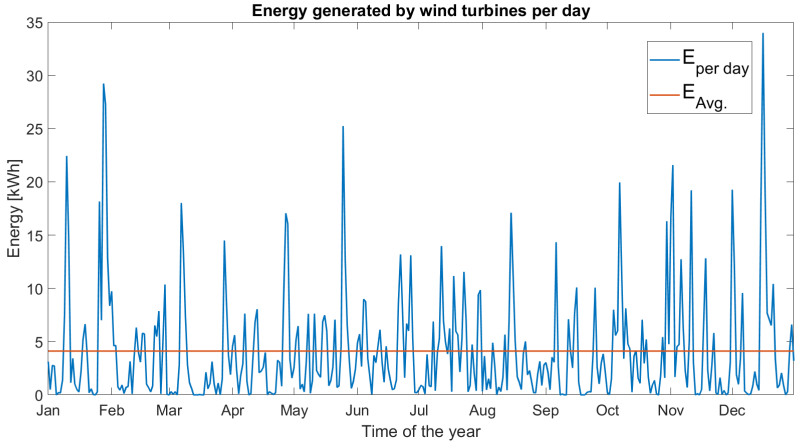


**Figure 5.2:** Estimated Production from wind turbines, along with the average WT production, both per day, in 2010.

The average production from SPV in 2010 was $E_{SPV}$ = 1.76kWh per day. But the variations for solar energy production is more concentrated to the summer

months, as figure 5.3 depicts. This is to be expected, as the sun is below the horizon from Novemver $25^{th}$, until January $17^{th}$ in Alta.

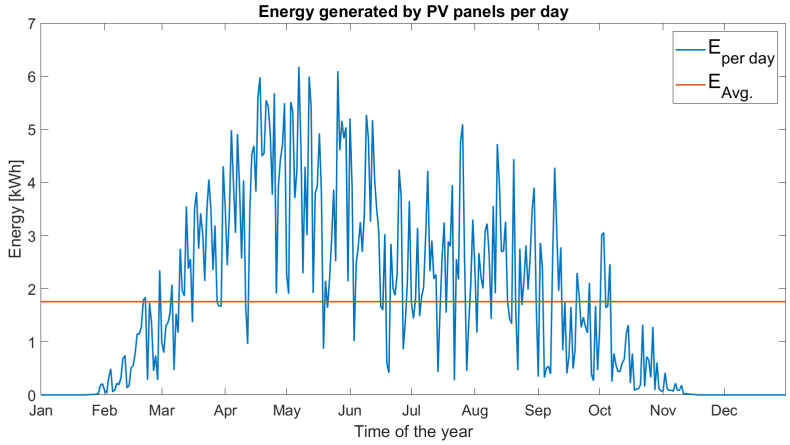


**Figure 5.3:** Estimated production from PV panels per day, and average daily production, in 2010.

Figure 5.4 shows the daily average BP capacity. Can see that the drops in capacity is concentrated to the winter months. For the periods where the SPV panels produce most energy, the BP capacity stays high. But this is also the period where the temperature is highest. As the temperature dependent PL is set to only draw 20W while $T_a < 0^oC$, this is a more likely reason for the high BP capacity in the summer months.

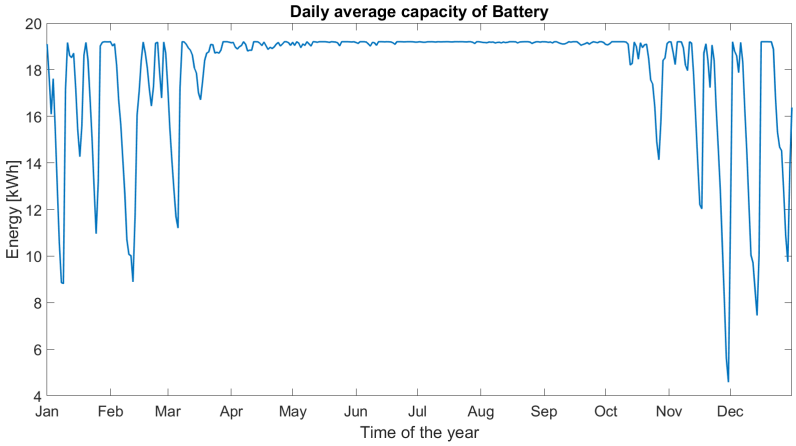


**Figure 5.4:** Daily average capacity on the battery bank as estimated in 2010.

Figures 5.5 and 5.6 shows daily total energy supplied for the temperature dependent PL and DL, respectively. The average daily energy demand for the PL is 1.37kWh. That is lower than the average production from both WT and

SPV panels. The DL gets the energy which is left over from the HRES after the PL have been supplied, if the BP is at full capacity. The average energy supply to the DL was 3.98kWh per day, in 2010. Can see from figure 5.6 that the DL gets a lot of energy at the same time as the WT production is high. And also more steady supply in the months in and around summer.

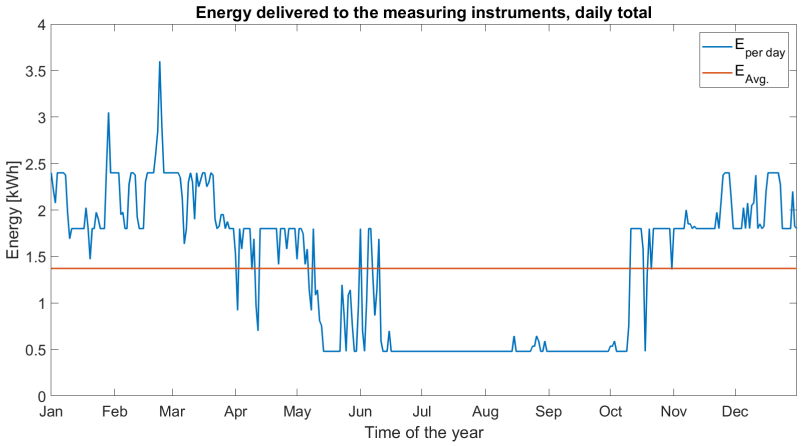


**Figure 5.5:** Estimated energy delivered to the PL through 2010, with temperature dependency.

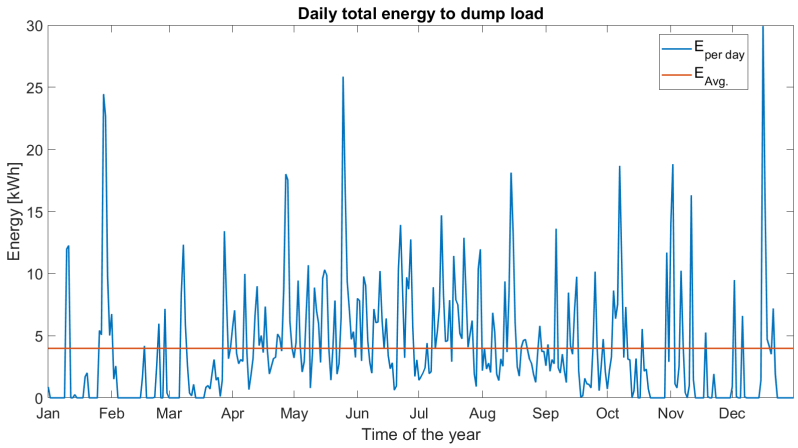


**Figure 5.6:** Estimated energy delivered to DL, with varialble PL, in 2010.

Figures 5.7, 5.8 and 5.9, shows the daily average BP capacity, the daily total energy supplied to the PL, and DL, respectively. In these figures the PL demands a constant high load of $150W$. As energy delivered to the PL should depict a constant line, the graph drops indicates shortage of power supply. Even though the PL is constantly high, there is still energy supplied to the dump load, as depicted in figure 5.9, with an average supply of 1.67kWh per day.

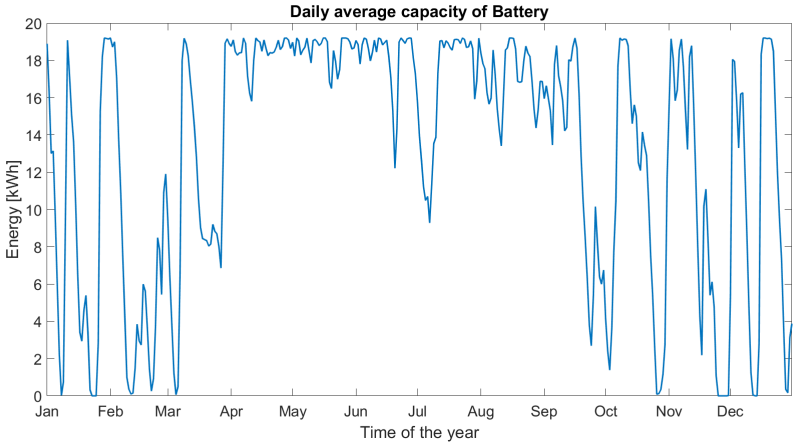


**Figure 5.7:** Estimated dalily average of battery with constant PL profile, $P_{PL} = 150W$, in 2010.

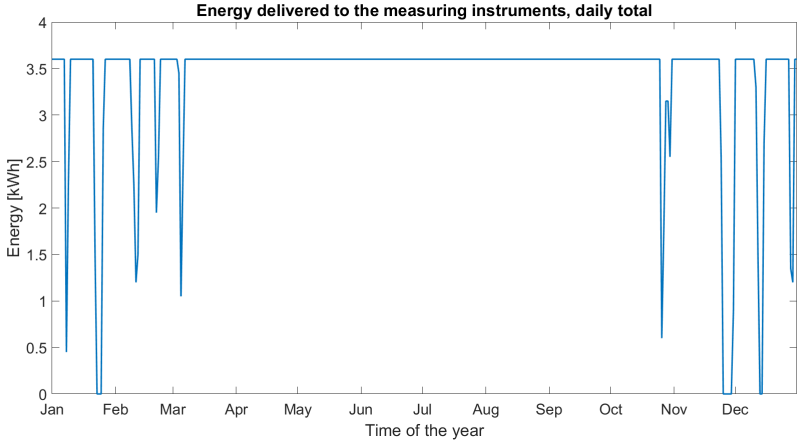


**Figure 5.8:** Energy delivered to PL with $P_{PL} = 150W$. Where the graph goes down to zero, shows shortage of power supply to PL, 2010.

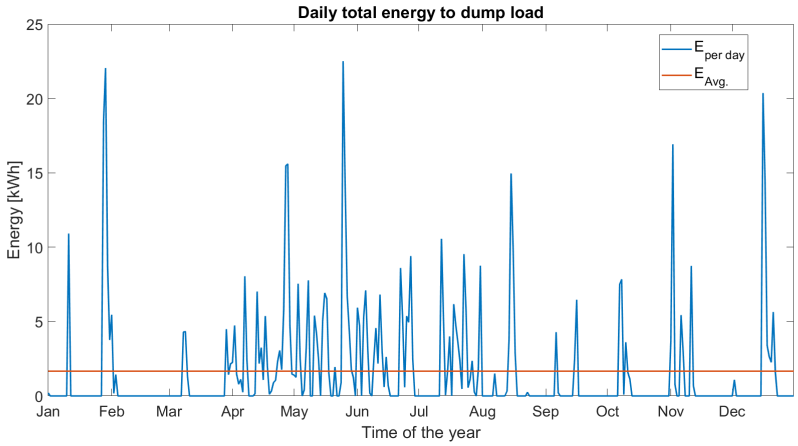


**Figure 5.9:** Energy delivered to DL with $P_{PL,C} = 150W$, in 2010.

## 5.2 Optimal production

Table 5.2 shows the results from the simulations with optimally mounted SPV pannels, scenario 2. The table shows that also this system can give steady power supply to the weather station, as the LOLP is zero with a temperature dependent PL. But the station will be down 5% of the time with a constant high PL.

**Table 5.2:** Results for system with optimally angled SPV panels, with model data from 2010.

| Parameters | Short name | Unit | Value |
|---|---|---|---|
| Total energy production | $E_{tot}$ | kWh | 2377.3 |
| Energy production from WT | $E_{WT}$ | kWh | 1499.7 |
| Energy production from PV | $E_{PV}$ | kWh | 877.7 |
| Capacity factor for WT | $C_{WT}$ | % | 9.65 |
| Capacity factor for PV | $C_{PV}$ | % | 9.63 |
| Energy delivered to primary load, with variable PL | $E_{PL}(T)$ | kWh | 500.6 |
| Energy delivered to dump load, with variable PL | $E_{DL}(T)$ | kWh | 1674.5 |
| Loss of load probability, with variable PL | LOLP | % | 0 |
| Energy delivered to primary load, with constant PL | $E_{PL,C}$ | kWh | 1248.3 |
| Energy delivered to dump load, with constant PL | $E_{PL,C}$ | kWh | 817.2 |
| Loss of load probability, with constant PL | LOLP | % | 5.00 |

## 5.3 All SPV panels on south-east wall

Table 5.3 shows the results from the simulations with all SPV panels on the south-east wall, scenario 3. Can see that the SPV energy production have an increase here compared to scenario 1. This scenario is also suitable for a temperature dependent PL, as the LOLP is equal to zero. But it cannot deliver steady supply for a constant high PL, as the LOLP 5.47%.

**Table 5.3:** Results with all SPV panels placed on the south-east wall, with model data from 2010.

| Parameters | Short name | Unit | Value |
|---|---|---|---|
| Total energy production | $E_{tot}$ | kWh | 2160.7 |
| Energy production from WT | $E_{WT}$ | kWh | 1499.7 |
| Energy production from PV | $E_{PV}$ | kWh | 661.0 |
| Capacity factor for WT | $C_{WT}$ | % | 9.65 |
| Capacity factor for PV | $C_{PV}$ | % | 7.26 |
| Energy delivered to primary load, with variable PL | $E_{PL}(T)$ | kWh | 500.6 |
| Energy delivered to dump load, with variable PL | $E_{DL}(T)$ | kWh | 1468.6 |
| Loss of load probability, with variable PL | LOLP | % | 0 |
| Energy delivered to primary load, with constant PL | $E_{PL,C}$ | kWh | 1242.2 |
| Energy delivered to dump load, with constant PL | $E_{PL,C}$ | kWh | 618.9 |
| Loss of load probability, with constant PL | LOLP | % | 5.47 |

## 5.4 Only wind turbines

Table 5.4 shows the results from simulations of the system with only WTs, scenario 4. It shows that 4 WTs are needed to meet the energy demand of a temperature dependent PL, with original BP size. But by doubling the BP, the original 2 WTs can supply a temperature dependent PL. The energy production is to variable to supply a constant high PL, as neither 4 WTs or a doubling of the BP capacity brings the LOLP to zero.

**Table 5.4:** Results for system with only wind turbines, with model data from 2010.

| Parameters | Short name | Unit | Value |
|---|---|---|---|
| Energy production from WT, with 2 turbines | $E_{2xWT}$ | kWh | 1499.7 |
| Capacity factor for WT | $C_{WT}$ | % | 9.65 |
| Energy delivered to primary load, with variable PL | $E_{PL}(T)$ | kWh | 489.0 |
| Energy delivered to dump load, with variable PL | $E_{DL}(T)$ | kWh | 856.6 |
| Loss of load probability, with variable PL | LOLP | % | 1.54 |
| Energy delivered to primary load, with constant PL | $E_{PL,C}$ | kWh | 1022.1 |
| Energy delivered to dump load, with constant PL | $E_{DL,C}$ | kWh | 213.4 |
| Loss of load probability, with constant PL | LOLP | % | 22.21 |
| Energy production from WT, with 3 turbines | $E_{3xWT}$ | kWh | 2249.5 |
| Energy delivered to primary load, with variable PL | $E_{PL}(T)$ | kWh | 495.1 |
| Energy delivered to dump load, with variable PL | $E_{DL}(T)$ | kWh | 1558.2 |
| Loss of load probability, with variable PL | LOLP | % | 0.74 |
| Energy delivered to primary load, with constant PL | $E_{PL,C}$ | kWh | 1223.3 |
| Energy delivered to dump load, with constant PL | $E_{DL,C}$ | kWh | 715.4 |
| Loss of load probability, with constant PL | LOLP | % | 6.91 |
| Energy production from WT, with 4 turbines | $E_{4xWT}$ | kWh | 2999.4 |
| Energy delivered to primary load, with variable PL | $E_{PL}(T)$ | kWh | 500.6 |
| Energy delivered to dump load, with variable PL | $E_{DL}(T)$ | kWh | 2260.3 |
| Loss of load probability, with variable PL | LOLP | % | 0 |
| Energy delivered to primary load, with constant PL | $E_{PL,C}$ | kWh | 1307.0 |
| Energy delivered to dump load, with constant PL | $E_{DL,C}$ | kWh | 1377.1 |
| Loss of load probability, with constant PL | LOLP | % | 3.85 |
| $E_{2xWT}$, but with double BP | $E_{2xWT}$ | kWh | 1499.7 |
| Energy delivered to primary load, with variable PL | $E_{PL}(T)$ | kWh | 500.6 |
| Energy delivered to dump load, with variable PL | $E_{DL}(T)$ | kWh | 846.2 |
| Loss of load probability, with variable PL | LOLP | % | 0 |
| Energy delivered to primary load, with constant PL | $E_{PL,C}$ | kWh | 1141.3 |
| Energy delivered to dump load, with constant PL | $E_{PL,C}$ | kWh | 99.2 |
| Loss of load probability, with constant PL | LOLP | % | 13.14 |

## 5.5 Only SPV panels

Table 5.5 shows the results of senario 5, where a system was simulated with only SPV panels. It shows how large the BP needs to be if this system was to be implemented. Without taking self-dischargeing of BP into account, the BP would have to be 15 times larger than originally planned, as in scenario 1.

**Table 5.5:** Results for system with only SPV, with data from July 2010 until July 2011, and LOLP for different sizes of the BP.

| Parameters | Short name | Unit | Value |
|---|---|---|---|
| Average energy production from SPV over the seven years | $E_{PV_{avg.}}$ | kWh | 650.3 |
| Capacity factor for PV | $C_{PV}$ | % | 7.14 |
| LOLP, with a battery capacity of 19.2 kWh | $LOLP_{1xBP}$ | % | 33.46 |
| LOLP, with a battery capacity of 96 kWh | $LOLP_{5xBP}$ | % | 22.84 |
| LOLP, with a battery capacity of 192.0 kWh | $LOLP_{10xBP}$ | % | 11.23 |
| LOLP, with a battery capacity of 268.8 kWh | $LOLP_{14xBP}$ | % | 1.69 |
| LOLP, with a battery capacity of 288.0 kWh | $LOLP_{15xBP}$ | % | 0 |

## 5.6 Comparing scenarios with different placement of SPV panels

Table 5.6 shows a comparison of the first three scenarios. Can see from the table that with a temperature dependent PL, all systems managed to fully supply the energy demand with data from 2010, as all LOLPs are zero. The extra power production in scenario 2 and 3, compared to scenario 1, was all delivered to the DL, in the case with a variable PL. With a constant high PL, none of the systems managed to fully deliver the power damand from the PL, as all LOLPs are higher than zero. In case of both SPV energy production, and LOLP for high constant PL, scenario 2 is better than both of the other two scenarios. Scenario 3 has higher production, and lower LOLP, than the other two. Scenario 3 has higher production and lower LOLP than scenario 1.

**Table 5.6:** Comparing results from the three simulations with both WTs and SPVs in the HRES, in 2010.

| **Parameters** | **Short name** | **Scenario 1** | **Scenario 2** | **Scenario 3** |
|---|---|---|---|---|
| Energy production [kWh] | $E_{tot}$ | 2140.4 | 2377.3 | 2160.7 |
| | $E_{WT}$ | 1499.7 | 1499.7 | 1499.7 |
| | $E_{SPV}$ | 640.7 | 877.7 | 661.0 |
| Capacity factor [%] | $C_{WT}$ | 9.65 | 9.65 | 9.65 |
| | $C_{SPV}$ | 7.03 | 9.63 | 7.26 |
| Energy delivered | $E_{PL}(T)$ | 500.6 | 500.6 | 500.6 |
| for variable PL [kWh] | $E_{DL}(T)$ | 1453.7 | 1674.5 | 1453.7 |
| LOLP [%] | | 0 | 0 | 0 |
| Energy delivered | $E_{PL,C}$ | 1239.0 | 1248.3 | 1242.2 |
| for constant PL [kWh] | $E_{DL,C}$ | 608.1 | 817.2 | 618.9 |
| LOLP [%] | | 5.71 | 5.00 | 5.47 |

# /6

# Discussion and conclusion

The weather data in section 4.1, show that both solar radiation and wind speed is lower for 2010, than for sourounding years. As such the results in the different scenarios can be seen as a minimum yearly production. Thus what works in these results for 2010, will also work with most other years, given that there is accuracy in the data used.

Four SPV panels produce enough energy to be the only source for a temperature dependent PL. But then the battery BP needs to increase, as there is no SPV energy production in the polar night. The polar night is also the period with lowest temperature, so it's here the energy is needed the most. As the results from senario 5 shows, the BP would have to be fifteen times higher than in the planned scenario. The simulations was also done without taking self-discharge of the battery into consideration. The battery used as reference in the simulations were stated to have a low self-discharge[14]. but some energy will be lost to self-discharge, so in reality the BP would need to be even bigger. As the weight of the planned BP was 504kg, fifteen times that would be a battery package weighing 7560kg. That would be an impractical battery size, both to transport to, and store inside NO.

A system with only WTs, as simulated in scenario 4, could work with some modifications. Wind energy production is more evenly distributed through the year than solar energy production is, as shown in figures 5.2 and 5.3. But wind energy production still fluctuates through the year, and there can be longer periods without any or sufficient production. As shown in table 5.4,

four turbines had to be installed to make the LOLP go down to zero, with a temperature dependent PL. For a system with WTs as the only energy source, it would then be easier to increase the BP package, as it would only need to double to meet the supply demand from the PL.

A HRES combining both wind and solar energy will eliminate some of the fluctuations in the separate resources. A such system is better suited to optimize the power supply for the PL. Scenarios 1, 2, and 3 was simulated as HRESs with two WTs and four SPV panels, with a BP. All three scenarios were able to give steady supply for the temperature dependent PL. As it was planned to mount the SPV panels on the south-west and south-east walls, two on each, the results from the simulations show that there are better ways to set up the system. Using a ground mounting structure to mount the SPV panels in optimal angles, the HRES would be able to deliver more steady supply to a higher PL, as shown in table 5.6 for scenario 2. As it was assumed that reflection from snow wasn't included in the in-plane irradiance data, SPV panels mounted at $90^o$ slope, would recieve more reflected irradiation from snow, than the results estimated. That could make the differences between scenario 2 and scenario 1 and 3 smaller.

To get as much power as possible from the WTs, it's important that they are placed such that one turbine doesn't shade the other from the wind. The wind roses in figures 4.2 and 4.3, show that the highest wind speeds come from the south and from the west of Halddetoppen. So the WTs should be placed such that a horizontal line through their towers, goes in the south-west north-east direction.

In conclusion it was found that wind energy can manage alone, but as the wind speed varies much through the year, it is better to use both wind and solar energy in a HRES. A system with only SPV panels would be impractical as it would need a large BP. The HRES planned to be installed was estimated to give sufficient power supply to the PL. But it was found better solutions to install the SPV panels for an optimal energy production.

# 7

# Future work

As the weather station gets installed, and measured data become available, the simulations can be redone with the measured data as input. The results in this thesis can also be compared to the production and operation of the installed HRES. Other scenarios can also be simulated to find higher production. A scenario with a one or two axis tracking system for the SPV panels would increase the energy production as the panles would always face the sun, as long as the sun is above the horizon. And as there is midnight sun in Alta, the SPV panels could potentially produce power continously through the polar day.

# Bibliography


[1] Dhaker Abbes, André Martinez, and Gérard Champenois. Life cycle cost, embodied energy and loss of power supply probability for the optimal design of hybrid power systems. *Mathematics and Computers in Simulation*, 98:46–62, 2014.

[2] Dhaker Abbes, André Martinez, Gérard Champenois, Jean Paul Gaubert, and Riad Kadri. Estimation of wind turbine and solar photovoltaic energy using variant sampling intervals. In *Proceedings of 14th International Power Electronics and Motion Control Conference EPE-PEMC 2010*, pages T12–28. IEEE, 2010.

[3] Apogee. Apogee instruments - owner's manual pyranometer models sp-510 and sp-610. 2018.

[4] Binayak Bhandari, Shiva Raj Poudel, Kyung-Tae Lee, and Sung-Hoon Ahn. Mathematical modeling of hybrid renewable energy system: A review on small hydro-solar-wind power generation. *international journal of precision engineering and manufacturing-green technology*, 1(2):157–173, 2014.

[5] Thies clima. Wind transmitter "first class" advanced x. 2017.

[6] Tracy Dahl. Camp raven renewable energy system. 2004.

[7] MK Deshmukh and SS Deshmukh. Modeling of hybrid renewable energy systems. *Renewable and sustainable energy reviews*, 12(1):235–249, 2008.

[8] Said Diaf, Gilles Notton, M Belhamel, M Haddadi, and Alain Louche. Design and techno-economical optimization for hybrid pv/wind system under various meteorological conditions. *Applied Energy*, 85(10):968–987, 2008.

[9] Yinke Dou, Guangyu Zuo, Xiaomin Chang, and Yan Chen. A study of a standalone renewable energy system of the chinese zhongshan station in

antarctica. *Applied Sciences*, 9(10):1968, 2019.

[10] Ajai Gupta, RP Saini, and MP Sharma. Modelling of hybrid energy system—part i: Problem formulation and model development. *Renewable Energy*, 36(2):459–465, 2011.

[11] AK 99775 Institute of Arctic Biology 902 N Koyukuk Dr University of Alaska Fairbanks Fairbanks. Imnavait creek power and communications system.

[12] Gill Instruments. Windsonic m user manual, ultrasonic anemometer. 2016.

[13] Mouna Lamnadi, Mourad Trihi, Abdelkader Boulezhar, Badre Bossoufi, et al. Optimal design of stand-alone hybrid power system using wind and solar energy sources. *International Journal of Energy Technology and Policy*, 15(2/3):280–300, 2019.

[14] Haze Battery Company Ltd. 6 and 12 volt monobloc gel range. pages 1–12, 2012.

[15] Marlec Engineering Co Ltd. Rutland fm1803-2 furlmatic windcharger data sheet. pages 1–3, 2007.

[16] Gilles Notton, Christian Cristofari, Michel Mattei, and Philippe Poggi. Modelling of a double-glass photovoltaic module using finite differences. *Applied thermal engineering*, 25(17-18):2854–2877, 2005.

[17] Ltd. Perlight Solar Co. Perlight solar plm-270p-60 series data sheet. pages 1–2, 2018.

[18] 2001-2017 PVGIS (c) European Communities. Pvgis.

[19] NH v Reich, WGJHM Van Sark, EA Alsema, RW Lof, REI Schropp, WC Sinke, and WC Turkenburg. Crystalline silicon cell performance at low light intensities. *Solar Energy Materials and Solar Cells*, 93(9):1471–1481, 2009.

[20] Tatsuo Saga. Advances in crystalline silicon solar cell technology for industrial mass production. *npg asia materials*, 2(3):96, 2010.

[21] Chetan Singh Solanki. *Solar photovoltaics: fundamentals, technologies and applications*. PHI Learning Pvt. Ltd., 2015.

[22] Kine Solbakken, Bilal Babar, and Tobias Boström. Correlation of wind and solar power in high-latitude arctic areas in northern norway and svalbard.

*Renewable Energy and Environmental Sustainability*, 1:42, 2016.

[23] David A Spera et al. *Wind turbine technology: fundamental concepts of wind turbine engineering*, volume 3. ASME press New York, 1994.

[24] NRG Systems. Nrg 200p wind vane spesifications. 2016.

[25] Vaisala. User's guide vaisala anemometer waa151. 2002.

[26] HX Yang, L Lu, and J Burnett. Weather data and probability analysis of hybrid photovoltaic–wind power generation systems in hong kong. *Renewable Energy*, 28(11):1813–1824, 2003.